Nuclear Instruments and Methods in Physics Research A 625 (2011) 47–56

Contents lists available at ScienceDirect

Nuclear Instruments and Methods in Physics Research A

journal homepage: www.elsevier.com/locate/nima

Technical Notes

Calibration of an electron volt neutron spectrometer

J. Mayers *, M.A. Adams

ISIS Facility, Rutherford Appleton Laboratory, Chilton, Didcot, Oxfordshire OX11 0QX, UK

ARTICLE INFO

Article history:
Received 9 September 2010
Accepted 22 September 2010
Available online 15 October 2010

Keywords:
Neutron detectors momentum distributions

ABSTRACT

The procedure for calibrating the VESUVIO eV neutron spectrometer at the ISIS neutron source is described. VESUVIO is used primarily to measure the momentum distribution n(p) of atoms, by inelastic scattering of very high energy (5–150 eV) neutrons. The results of the calibrations show that measurements of n(p) in atoms with masses lower than 16 amu can be measured with a resolution width ~25% of the intrinsic peak widths in the current instrument configuration. Some suggestions as to how the instrument resolution could be significantly improved are made.

1. Introduction

The main purpose of this paper is to describe the procedures used to calibrate the VESUVIO spectrometer at the ISIS neutron source. VESUVIO is used primarily to measure the momentum distributions of atoms, by inelastic scattering of neutrons with energies in the range 5–150 eV. This technique is known as neutron Compton scattering (NCS) by analogy with the older technique of Compton scattering, used to measure the momentum of electrons by scattering of high energy photons. Both techniques rely upon the fact that at sufficiently high momentum transfers in any collision process, the impulse approximation (IA) is accurate [1]. In NCS measurements the IA implies that the neutron scatters from a single atom, with conservation of kinetic energy and momentum of the neutron+atom. Hence the neutron inelastic scattering cross-section is related in a simple way to the momentum distribution of the atoms. Details of the technique and the data analysis used are given in Ref. [2]. Examples of recent measurements made using VESUVIO are given in Refs. [3–9].

VESUVIO is a unique instrument—other inelastic neutron spectrometers operate at energy transfers 1–4 orders of magnitude lower. Hence many of the calibration procedures used are also unique. An earlier paper [10] has already been published on this topic. However the instrument has recently been rebuilt with a different detection system and experimental geometry. Most of the calibration procedures described in this report are therefore new.

Section 2 contains a description of the current VESUVIO instrument and outlines the theory of the instrument resolution function. Section 3 discusses how the mean values of instrument parameters such as neutron path lengths, scattering angles and final energy are determined at forward angles. Section 4 discusses the measurement of the distributions of these parameters about their mean values—these distributions determine the resolution of VESUVIO. Section 5 describes the procedures used to calibrate the detectors at back-scattering. Section 6 contains calculations of the resolution components of VESUVIO in momentum space for different atomic masses. Section 7 contains a summary and suggestions of ways in which the instrument resolution could be significantly improved.

2. Description of VESUVIO

2.1. Instrument layout

VESUVIO is illustrated schematically in Fig. 1. There is a standard ISIS incident beam monitor (S1) and a transmitted beam monitor (S2) composed of beads of ^{6}Li doped scintillator glass.

At forward scattering there are 64 detectors (S135–S198) composed of cerium doped Yttrium Aluminium Perovskite (YAP) scintillator gamma ray detectors [11–13]. These are arranged in almost vertical columns of 8 detectors, with 4 above and 4 below the horizontal plane passing through the sample centre. Each detector element is 8 cm in height, 2.5 cm in width and of thickness ~0.6 cm. Gold foils are placed on the surface of the detector and the gamma rays emitted due to the absorption resonance at ~4.9 eV are detected. A differencing technique [14] is used to remove the background and sharpen the energy resolution. The final neutron energy is fixed at 4897 meV, with an energy resolution function which is well described by a convolution of a Lorentzian of half width at half maximum 24 meV and a Gaussian with standard deviation 73 meV [15] (see Section 3.1).

At back scattering there are 132 ^{6}Li doped glass scintillation neutron detectors (S3–S134). A double differencing technique using two thicknesses of gold foils [16] is used to define the final energy as 4897.3 meV. At back scattering the resolution is again almost

* Corresponding author.
E-mail address: j.mayers@rl.ac.uk (J. Mayers).

0168-9002/$ - see front matter © 2010 Elsevier B.V. All rights reserved.
doi:10.1016/j.nima.2010.09.079

Gaussian, but with small wings. The resolution function fits accurately to a convolution of a Gaussian of standard deviation 74 meV and a Lorentzian of half width at half maximum (HWHM) 24 meV.

2.2. Resolution function of VESUVIO

As is the case with all inelastic instruments at ISIS, VESUVIO uses time of flight measurements to determine the momentum and energy transfer to the neutron in each scattering event. The data collection system assigns a time of flight t for each neutron to pass from source to detector. This is

$$t = \frac{L_0}{v_0} + \frac{L_1}{v_1} + t_0 \quad (1)$$

L_0 is the path length from source to sample, L_1 that from sample to detector, v_0 is the velocity of the incident neutron and v_1 that of the scattered neutron. t_0 is an offset due to delays in the electronic counting chain. On VESUVIO the values of L_0, L_1, v_1, t_0 and the scattering angle θ can be characterised by a mean value, with an associated distribution about the mean. Given these mean values and the assigned time of flight t, the incident velocity v_0 of each neutron detected can be determined from Eq. (1). Hence the momentum and energy change of the neutron can be determined for each event.

The distributions of the parameters L_0, L_1, v_1, t_0 and θ about their mean values determine the resolution function of the instrument. The distribution in L_0 is determined by the finite size of the moderator and sample. The distributions of L_1 and θ are determined by the moderator, sample and detector geometry. The uncertainty in v_1 is determined by the band-width of energies absorbed by the gold foil. The uncertainty in the value of t assigned to the neutron is determined by the time bin width and the stability of the electronics in the counting chain.

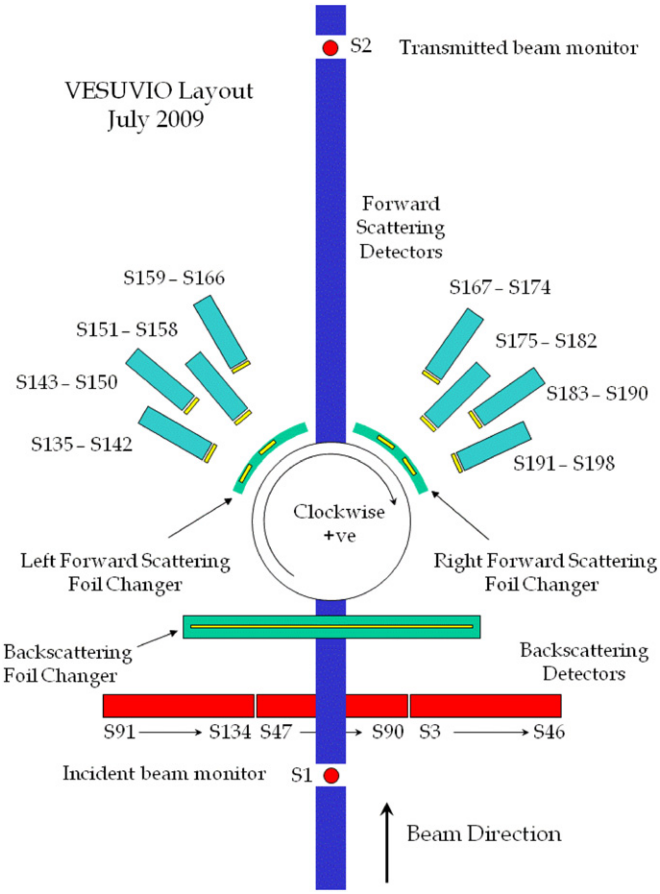

Fig. 1. Schematic diagram of the VESUVIO instrument. The spectrum numbers corresponding to the different detectors are shown. The positions of the foil changers used in the differencing measurements are also indicated in yellow. (For interpretation of the references to colour in this figure legend, the reader is referred to the web version of this article.)

3. Determination of mean instrument parameters

3.1. Determination of incident flight path L_0

The incident flight path is determined by placing a uranium foil at the sample position. Uranium has a series of sharp neutron resonance absorption peaks. When a neutron is absorbed by one of these resonances, gamma rays are emitted and these are registered by the YAP detectors at forward scattering. One of the 64 YAP time of flight spectra obtained is shown in Fig. 2.

When a neutron is absorbed by the foil, gamma rays are emitted, effectively instantaneously. These take a negligible time to pass from foil to detector. Hence the position in time of flight of the gamma ray peaks in Fig. 2 is determined by the time taken for neutrons to travel from source to the foil at the sample position. This is

$$t = \frac{L_0}{v_0} + t_0 \quad (2)$$

The parameters describing the absorption cross-section of neutrons in uranium are very accurately known [17]. Hence

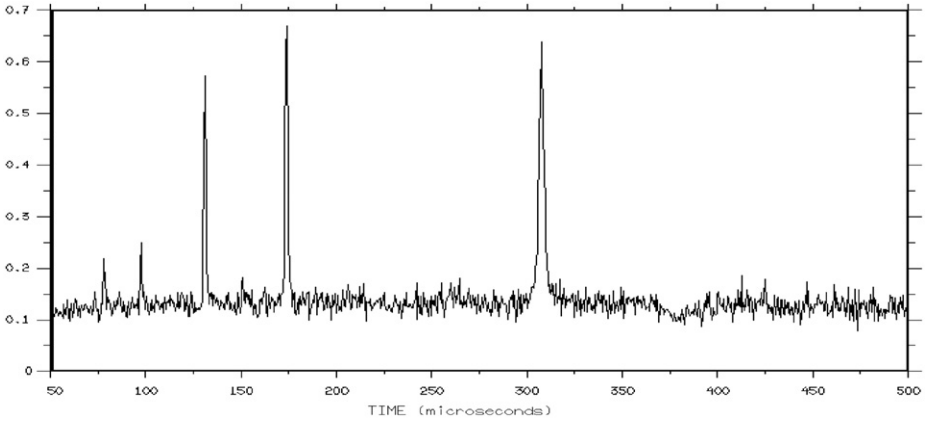

Fig. 2. Shows resonance peaks in the time of flight spectrum produced in a single detector with a U foil at the sample position. The U foil data was divided by the scattering from a Pb sample to remove the spectrum shape.

given the measured foil thickness, the absorption in the foil can be accurately calculated. The foil thickness was determined by weighing the foils and measuring their area. This measured thickness was used to calculate the absorption of the foils as a function of energy at 293 K, using the algorithm of Ref. [16]. The peak shapes are dominated by thermal broadening and are quite close to Gaussian in shape. The calculated foil absorption peaks were fitted to Gaussians to determine the neutron energy corresponding to the peak centres. The values obtained for the resonance energies and the standard deviation of the fitted Gaussians ΔE_R are listed in Table 1. (The full width at half height is $2.35\Delta E_R$.)

The measured peaks in the data shown in Fig. 2 are also fitted to Gaussians in t. The final column of Table 1 gives the fitted positions t_R of the peaks in the time of flight data, averaged over the 64 YAP detectors. It follows from Eq. (2) that if t_R is plotted as a function of $1/v_R$, the value of L_0 is obtained as the gradient and t_0 as the intercept. Fig. 3a shows values of L_0 obtained by this method from linear least-squares fitting of the three fitted peak positions in time of flight for the 64 YAP detectors. All detectors give the same value of L_0 to within $\sim$1 cm. Fig. 3b shows the corresponding values of t_0. The error bars in the plots are the standard error in the linear fit to the three values.

Table 1
Parameters defining the uranium absorption peaks used in the calibration. These were calculated for a foil with1.2081 E20 atoms/cm^2. E_R is the position of the Gaussian fit to the calculated absorption. ΔE_R is the corresponding standard deviation of the Gaussian. v_R is the velocity of a neutron with energy E_R. t_R is the fitted position in time of flight of the peaks shown in Fig. 2, averaged over the 64 YAP detectors. The quoted error is the standard error in the mean over the 64 YAP detectors.

E_R (meV)	ΔE_R (meV)	v_R (m/s)	t_R (μs)
6672	52.4	35725	307.70 ± 0.01
20874	91.7	63190	173.80 ± 0.01
36684	133.6	83768	131.00 ± 0.01

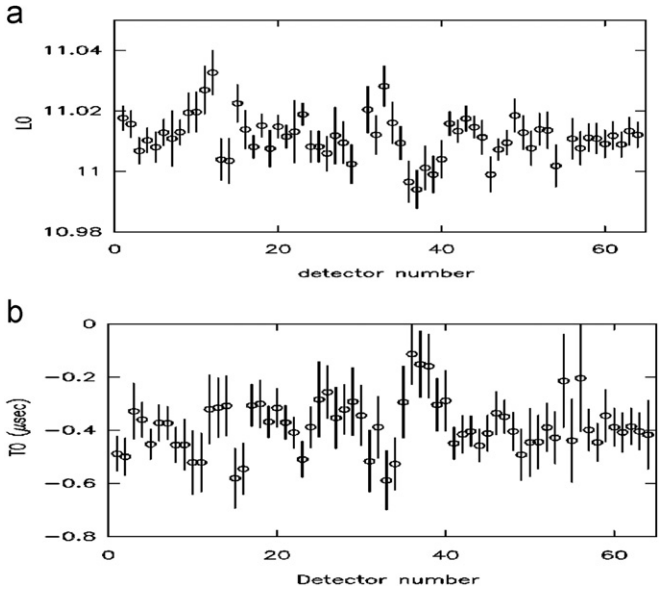

Fig. 3. (a) Values of L_0 (m) obtained from fitting the U resonance positions on the 64 YAP detectors at forward scattering angles. The mean of the 64 detectors is $L_0 = 11.005 \pm 0.001$ m. (b) Shows values of t_0 (μs) obtained from fitting the U resonance positions on the 64 YAP detectors via the procedure described in the text. The mean is $t_0 = -0.40 \pm 0.02$ μs.

The incident flight path, obtained from the mean of the values obtained from the 64 YAP detectors is $L_0 = 11.005$ m, with a standard error in the mean of ± 0.001 m. The mean value of the time delay is $t_0 = -0.40$ μs with a standard error of ± 0.02 μs. The negative value of t_0 implies that the time zero pulse provided by the ISIS source arrives at the detector electronics after the mean time of emission of the neutrons, presumably due to electronic delays in the counting chain.

3.2. Determination of the final energy E_1

The mean final energy E_1 of the neutron was determined using the ^{6}Li doped back-scattering detectors. Fig. 4 shows a typical time of flight spectrum collected on one of the134 ^{6}Li detectors with the standard VESUVIO lead calibration sample. This is a 2 mm thick slab, which scatters about 7% of the beam. Lead is a good calibration standard for NCS measurements for a number of reasons. It has a low Debye temperature (90 K) and hence has a momentum distribution which is closely Gaussian. The low Debye temperature also implies that at room temperature the impulse approximation is very accurate at the momentum transfers accessed on VESUVIO [18]. Partly due to its low Debye temperature and partly to its high mass the lead peak is also significantly narrower than the resolution function of the instrument, as can be seen in Figs. 4 and 6. The scattering is also very close to isotropic and elastic due to the high mass of lead and the correspondingly small recoil.

A typical fit of a Voigt function (a convolution of a Lorentzian and a Gaussian) to the time of flight lead data is also shown in Fig. 4 as the red line. It can be seen that the shape of the resolution function is accurately captured by this two parameter fit. From the fitted position in time of flight of this peak the final energy can be determined by the following argument.

Since the impulse approximation is very accurate for scattering from lead at room temperature [18]. The ratio of the final and incident neutron velocities of neutrons detected at the peak centres (corresponding physically to an atom with zero momentum) is accurately fixed by conservation of kinetic energy and momentum of the neutron+atom as

$$\frac{v_1}{v_0} = \frac{\cos\theta + \sqrt{(M/m)^2 - \sin^2\theta}}{(M/m)+1} \tag{3}$$

where $M = 207.19$ amu is the mass of a lead atom, $m = 1.0087$ amu is the mass of the neutron and θ is the scattering angle.

The values of L_0, L_1, t_0 and θ can be calibrated very precisely on the ^{6}Li doped detectors, using the measured transmission of a

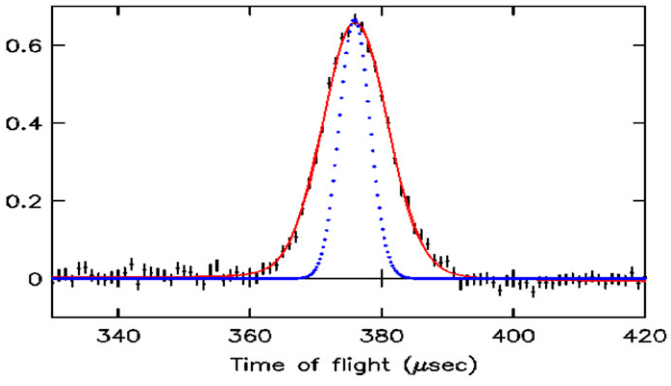

Fig. 4. The black points are a typical time of flight spectrum from one of the 132 ^{6}Li doped detectors (at $\sim$140°), with the lead calibration sample. The Voigt fit to the data is shown as the red line. The calculated width in t due to the momentum distribution of the lead atoms is shown as the blue dotted line. (For interpretation of the references to colour in this figure legend, the reader is referred to the web version of this article.)

uranium foil as described in Section 5. Hence using Eqs. (1) and (3), the value of v_1 and hence $E_1 = \frac{1}{2}mv_1^2$ can be determined for each detector from the fitted positions of the Pb peak in time of flight. The values of E_1 obtained from averages over the three backscattering banks are given in Table 2. The final row gives the average over all backscattering detectors and is the value used in data analysis.

The foil absorption was calculated for the measured gold foil thickness used on VESUVIO using the algorithm given in Ref. [16] and tabulated parameters from Ref. [17]. The calculated foil absorption is shown in Fig. 5, as black dots. The calculated absorption was fitted with a Voigt function and gave a value of $E_1 = 4906.4$ meV for the peak position. The fit is shown as the red line. A fit to the square of the absorption (this is the resolution function at forward scattering [15]) gave an identical value for E_1.

The quoted errors [17] on the parameters used give an error in the calculated peak position of $\pm \sim 10$ meV. The calculated value of 4906.3 thus agrees within error with the calibrated value of $E_1 = 4897.3$ meV. The calibrated value is preferred as should be more accurate—it is determined essentially by the tabulated values of the positions of uranium resonances, via the procedures described in Section 5. These are known much more accurately (to within $\pm \sim 1$ meV) [17] than those of gold.

3.3. Determination of final flight path L_1

The final flight path from sample to detector can also be determined from the lead calibration. The time of flight data in every YAP detector is fitted to a Voigt function after correcting for gamma background [19] and multiple scattering. [20]. Typical data and fit for a single YAP detector are shown in Fig. 6. Given the calibrated values of L_0, t_0 (Section 3.1), v_1 (Section 3.2) and θ (Section 3.4), L_1 can be determined using Eqs. (1) and (3). Values of L_1 determined in this way are shown for the 64 YAP detectors in Fig. 7. The error due to counting statistics in the calibrated value of L_1 for each detector is ~ 1 mm.

Table 2
The values of the mean final energy E_1 obtained from fitting lead data at backscattering. The errors are the standard error in the mean.

Detector bank	E_1 (meV)
S3–S46	4897.1 ± 0.7
S47–S90	4897.5 ± 0.7
S91–S134	4895.6 ± 0.8
S3–S134	4897.3 ± 0.4

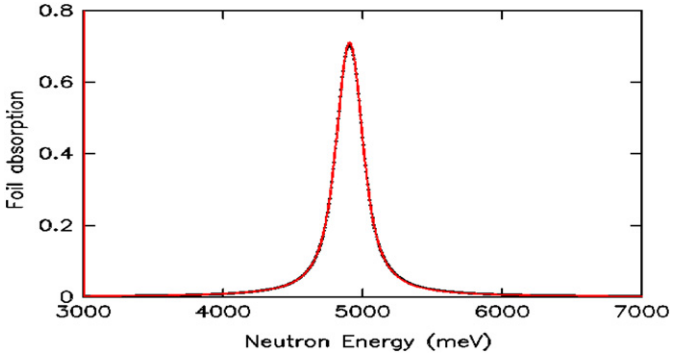

Fig. 5. Calculated foil absorption is shown as the black dots. The fit of a Voigt function is shown as the red line. The fitted peak position was 4906.3 meV. (For interpretation of the references to colour in this figure legend, the reader is referred to the web version of this article.)

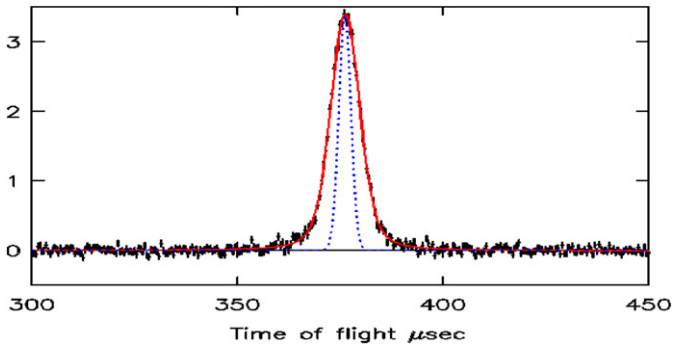

Fig. 6. Data from Pb in a single YAP detector (at $\sim 50^\circ$) after correction for gamma background and multiple scattering [20]. The data is shown in black with statistical errors. The red line is a fit to a Voigt function. The blue dotted line is the intrinsic width due to the calculated Pb momentum distribution at 290 K. (For interpretation of the references to colour in this figure legend, the reader is referred to the web version of this article.)

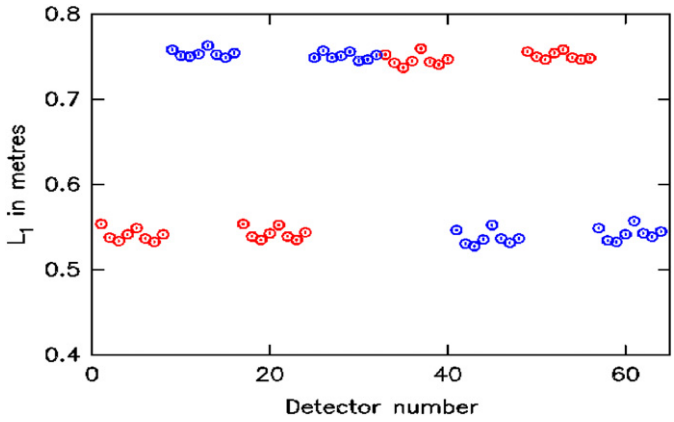

Fig. 7. Shows the values of L_1 in m determined for the 64 YAP detectors at forward angles.

3.4. Determination of the scattering angle

The YAP detectors are covered with a thin foil of cadmium which absorbs neutrons in the thermal region. The gamma ray emission associated with this absorption allows the detection of neutrons with energies < 200 meV. Scattering from Pb therefore produces Bragg peaks. A typical spectrum showing the 5 longest d-spacing Bragg peaks of Pb is shown in Fig. 8.

According to Bragg's law, the scattering angle is given by

$$2d\sin\theta = \lambda \tag{4}$$

The d-spacings for lead can be calculated from tabulated values of the lattice parameter. The neutron wavelength λ is determined by the time of flight at the peak centre and the calibrated values of L_0, L_1 and t_0 obtained via the procedures in Sections 3.2 and 3.3. Hence the scattering angle θ can be determined from Eq. (4).[1]

The positions of the 4 longest d spacing Bragg peaks in each of the 64 detectors were determined in the time of flight spectra using a cursor. The scattering angle is taken as the mean of the 4 values of

[1] Since the values of θ are required to determine E_1 and L_1 and vice versa, the procedure may seem inconsistent. However the values of E_1 and L_1 obtained depend only very weakly upon θ. More accurate values can be obtained by iteration. That is (1) Use estimated value of θ to determine E_1 and L_1. (2) With these values of E_1 and L_1, determine new value of θ. (3) With new value of θ re-determine E_1 and L_1, etc. The procedure converges with a single iteration.

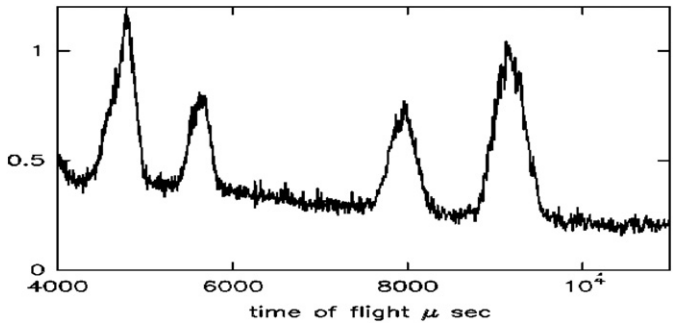

Fig. 8. The 5 longest d-spacing Bragg peaks from Pb at a scattering angle of 50°. The peak at ~4600 μs is the superposition of two peaks which are not resolved.

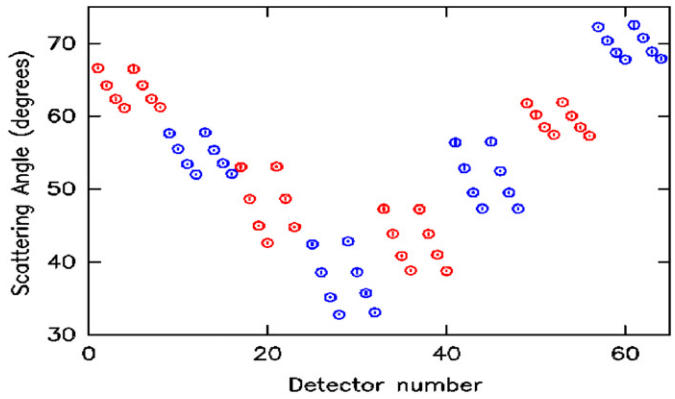

Fig. 9. Shows the values of the total scattering angle obtained from the calibration for the 64 YAP detectors.

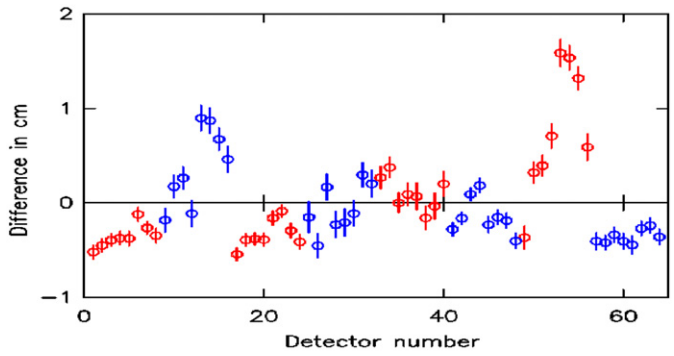

Fig. 10. Shows the difference in cm between values of L_1 obtained by the calibration procedure and a direct measurement (calibration—direct measurement).

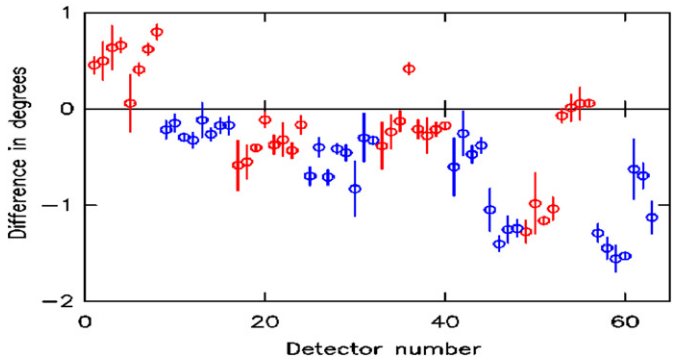

Fig. 11. Shows the difference in degrees between the scattering angle measured using neutrons and a direct measurement (neutron measurement—direct measurement).

θ determined from these positions. Fig. 9 shows mean values of θ determined by this method. The standard error in the mean of the 4 values is typically $\sim \pm 0.2^\circ$ for each detector.

The systematic change in scattering angle in banks of 4 detectors, which can be observed in Fig. 9, is due to the fact that the YAP detectors are in vertical columns of 4 above and below the horizontal plane containing the sample. As the distance of the detector from this plane increases, the scattering angle also increases.

3.5. Comparison with direct measurement

The positions of the detectors were also measured "directly" using a combination of steel rules and a straight edge that could rotate about the sample centre. From these measurements the total scattering angle θ and the final flight path L_1 can be determined and compared with those obtained by the calibration procedures given in Sections 3.1–3.4. The differences between the value of L_1 obtained by the calibration procedure and direct measurement are shown in Fig. 10, while the differences in the calibrated and directly measured scattering angles θ are shown in Fig. 11.

It can be seen that there is generally a good agreement between the direct measurement and the calibrated values. The lengths L_1 agree to within ~1 cm and the angles to within ~1°. The most probable origin of the discrepancies is a slight misalignment of detectors. This makes the determination of L_1 and θ by direct methods difficult, although these parameters can still be precisely determined by neutron calibration.

4. Determination of the instrument resolution

The resolution of the instrument is determined by the distributions of the instrument parameters t_0, L_0, L_0 and E_1 about their mean values.

4.1. Pulse width and uncertainty in the measurement of t

For energies > 1 eV on pulsed sources, the pulse width (that is the duration in time of the pulse of neutrons of a given energy) is inversely proportional to the incident neutron velocity [21]. Hence it can be characterised in terms of an uncertainty ΔL_0 in the incident flight path. The pulse width should be distinguished from the uncertainty Δt in the value of t assigned to the neutron, determined for example by the bin width chosen and by the limitations of the counting electronics.

The Gaussian fits to the resonance peaks shown in Fig. 2 give a width in t for each peak, in addition to the peak position ("widths" unless otherwise specified are the standard deviations of the fitted Gaussians). This width has components due to the intrinsic width of the absorption resonance, the uncertainty Δt with which t can be measured and the uncertainty ΔL_0 in the incident flight path (or equivalently the pulse width in time). It is assumed that all distributions are Gaussian, so that these widths add in quadrature. The fitted width in t (σ_{tot}) is therefore given by

$$\sigma_{tot}^2 = \frac{\Delta L_0^2}{v_R^2} + \Delta t_R^2 + \Delta t^2 \quad (5)$$

where

$$\Delta t_R = \frac{t_R}{2}\frac{\Delta E_R}{E_R} \tag{6}$$

is the intrinsic width of the absorption line. This was calculated using the values listed in Table 1. Calculated values of Δt_R and measured values of σ_{tot} are given for the three peaks in Table 3.

It follows from Eq. (5) that from a least squares fit of σ_{tot}^2 against $1/v_R^2$ the value of Δt can be determined from the intercept and ΔL_0 from the gradient. The values of ΔL_0 obtained for the 64 detectors by this procedure are shown in Fig. 12a. The values of Δt obtained are shown in Fig. 12b. The mean value $\Delta t = 0.37 \pm 0.02$ μs is determined partly by the bin width of 0.5 μs in the time of flight spectra and partly by any uncertainty due to electronic noise. The mean value of $\Delta L_0 = 2.1 \pm 0.2$ cm agrees well with the value (2.0 ± 0.2 cm) derived previously by measuring the transmission of a U foil. [10].

For an incident energy of 1 eV the FWHM of the pulse width given by calculations performed during the design phase of the moderators of ISIS [22] is ~1 μs. The calibrated value of ΔL_0 gives a value of ~1.5 μs at 1 eV. Given the assumptions in the analysis (in particular that the pulse shape is Gaussian), this agreement between measurement and calculation is satisfactory.

Table 3
E_R is the calculated energy at the centre of the uranium absorption line. v_R is the corresponding neutron velocity. Δt_R is the calculated width in t of the absorption line. σ_{tot} is average over the 64 YAP detectors of the fitted width in t. The quoted error is the standard error in the mean.

E_R (meV)	v_R (m/s)	Δt_R (μs)	σ_{tot} (μs)
6672	35725	1.21	1.38 ± 0.02
20874	63190	0.38	0.62 ± 0.01
36684	83768	0.24	0.51 ± 0.01

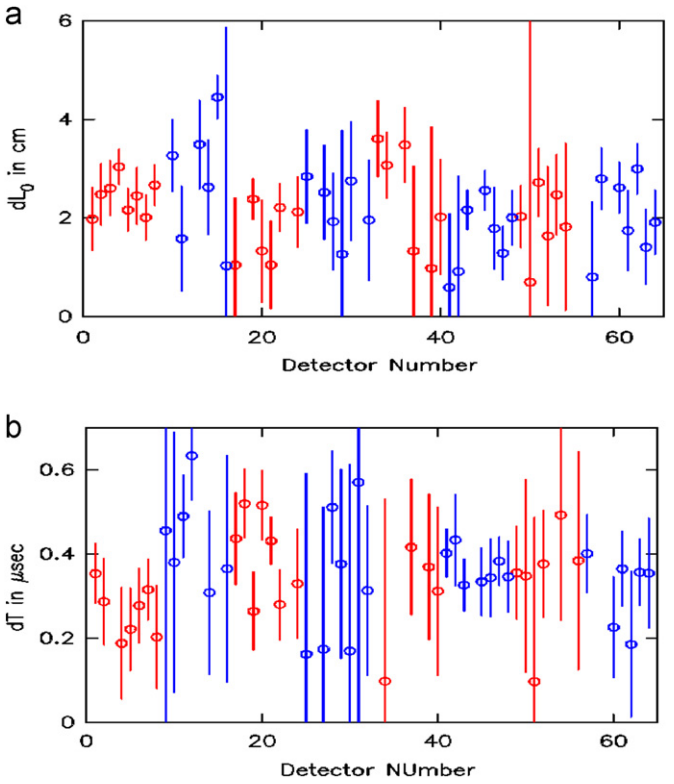

Fig. 12. (a) Values of ΔL_0 obtained as a function of detector number. The mean value is 2.4 ± 0.1 cm. (b) Values of Δt obtained from the calibration. The mean value was 0.37 ± 0.02.

4.2. Uncertainty in L_1

The uncertainty in L_1 is due to (a) the different possible positions that neutrons can be incident on the sample, due to the finite beam and sample size and (b) the different possible positions where they can be incident on the detector, due to the finite detector size. The spread of L_1 values was calculated by a Monte Carlo simulation using the known detector size. The VESUVIO beam is circular with a mean diameter of 4 cm and the calculation assumes a slab sample perpendicular to and covering the incident beam. The positions of the detectors in three dimensions, determined in Section 3, were used to define the geometry of the instrument. The calculated values of ΔL_1 (which was taken as the rms deviation from the mean of the events in the simulation) are shown in Fig. 13.

4.3. Uncertainty in E_1

The uncertainty in the final energy ΔE_1 is determined from the calibration run with the Pb sample. Data from a single YAP detector is shown in Fig. 6, together with the fit of a Voigt function. The width of the peak has two components: (i) by the intrinsic width due to the distribution of momenta of lead atoms in the sample—this is shown as the blue dotted line; (ii) the values of ΔL_0, Δt and ΔL_1 determined in Sections 4.1 and 4.2 and the distribution of scattering angles $\Delta\theta$, determined in Section 4.4 also contribute slightly to the width. However the energy resolution is the dominant contribution to the measured width with a lead sample (see Fig. 19e).

It is assumed that all contributions to the width other than that from the energy resolution give a Gaussian distribution in t. The quality of the fits shown in Figs. 4 and 6 shows that this assumption introduces no noticeable inaccuracies. Thus these contributions can be subtracted in quadrature from the fitted Gaussian component of the Voigt function to determine the Gaussian and Lorentzian components of the energy resolution function. The widths extracted from the fits were converted to an equivalent width in energy using Eq. (6). The fitted values of the Lorentzian component ΔE_{1L} and the Gaussian component ΔE_{1G} obtained from fitting are shown in Fig. 14a and b for the 64 YAP detectors.

The mean value of ΔE_{1L} was 24 ± 1 meV. The mean value of ΔE_{1G} was 73 ± 0.5 meV. The errors quoted are the standard error in the mean over 64 detectors. The individual values of ΔE_{1L} and ΔE_{1G} shown in Fig. 14a and b are stored in a resolution file which can be read by the analysis programs.

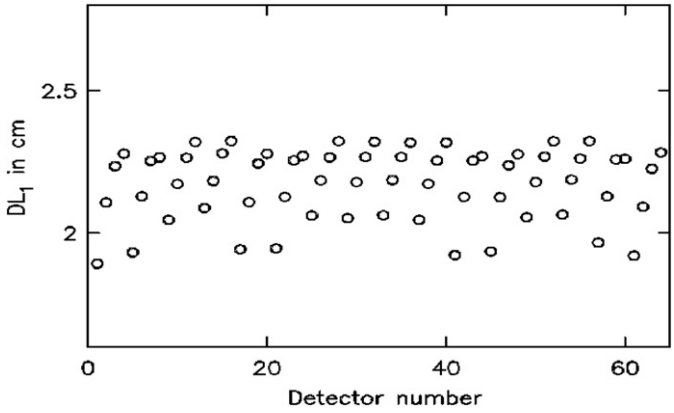

Fig. 13. Values of ΔL_1 calculated as a function of detector number. The mean value is 2.3 ± 0.2 cm.

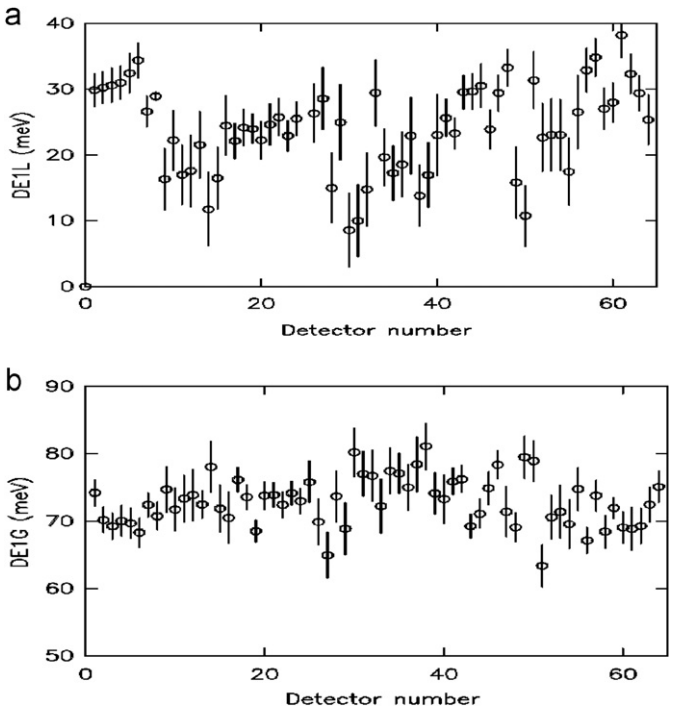

Fig. 14. (a) Values of the Lorentzian HWHM of the energy resolution function. Mean 24 ± 1 meV. (b) Values of the Gaussian SD of the energy resolution function. Mean $= 73 \pm 0.5$.

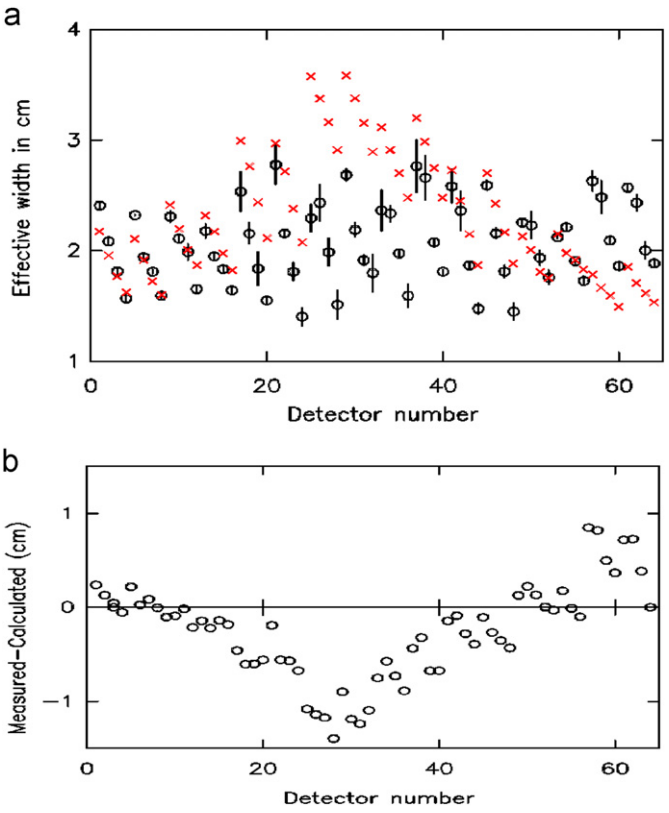

Fig. 15. (a) Values of DW determined by the calibration procedure described are shown as the black circles, with errors. Those calculated by Monte Carlo integration using the measured instrument geometry are shown as red crosses. (b) Difference between calculated and calibrated values of DW in cm. The largest differences occur at the lowest scattering angles (For interpretation of the references to colour in this figure legend, the reader is referred to the web version of this article.)

4.4. Uncertainty in angle

The uncertainty in scattering angle was determined by measuring the widths of the Bragg peaks obtained from the standard Pb calibration sample (see Fig. 8). The width of the peaks at forward scattering angles is totally dominated by the angular resolution of the detectors. Hence the range of neutron wavelengths in the peak is given by Eq. (4) as

$$\Delta\lambda = 2d\cos\theta\Delta\theta \tag{7}$$

It follows that

$$\frac{\Delta\lambda}{\lambda} = \frac{\Delta t_\theta}{t} = \frac{\Delta\theta}{\tan\theta} \tag{8}$$

where Δt_θ is the fitted Gaussian standard deviation of the peaks in t. The resolution of the detector can be defined in terms of an effective width DW, defined as

$$\mathrm{DW} = L_1\Delta\theta \tag{9}$$

Gaussian fits were made to the 3 highest order Bragg peaks in t for each spectrum and the values of $\Delta t_\theta/t$ were determined for each peak. DW was calculated as the mean of the 3 values obtained from the fitted values of $\Delta t_\theta/t$. Fig. 15a shows calibrated values of DW for all 64 detectors as the black circles. The error bars are the standard error in the mean of DW values calculated from the three fitted values of $\Delta t_\theta/t$. The figure also shows as red crosses the values of DW calculated by Monte Carlo integration using the measured instrument geometry. Fig. 15b shows the differences between the calibrated value of DW and the calculated values.

It can be seen that the qualitative agreement between calibration and calculation is good. The systematic variation in DW within a single column of groups of 4 detectors seen in the calibration is reproduced in the calculation. This variation is due to the fact that the detectors are in an almost vertical column and do not lie on the Debye–Scherrer cone. As the z value of a detector increases the deviation from the Debye–Scherrer cone increases, hence the angular resolution worsens. The differences between calibration and calculation are probably due to the difficulty of precisely defining the instrument geometry in the calculation. For example it is assumed that the plane of the detectors is perpendicular to the line joining the sample and detector centres. Any misalignment of the detectors will lead to an error in the calculated value of DW, although it will not affect the accuracy of the calibration.

It can be seen by examination of Figs. 15b and 9 that the largest deviations between calculation and calibration occur at the lowest scattering angles, where deviations of the detector geometry from the Debye–Scherrer cone produce the largest effects. Again this suggests that the difficulties of defining the exact detector geometry are responsible for the differences between calculation and measurement seen in Fig. 15b. As discussed above, this shows that a significant improvement of resolution could be obtained without any loss in count rate by a different detector geometry.

5. Calibration of the back-scattering detectors

The methods used to calibrate the back scattering detectors are very similar to those described in Sections 4 and 5 for the forward scattering detectors. However there are some differences due to the different methods for neutron detection used at backward (^{6}Li doped neutron detectors) and forward (YAP γ-ray detectors) angles. Many of the procedures in this section have already been described in Ref. [10]. The values of L_0 and ΔL_0 and are the same for both forward and back-scattering. Hence the values of these quantities derived in Sections 3.2 and 4.1 are used for all detectors. The procedure for defining the final energy and energy resolution has already been described in Sections 3.1 and 4.3.

5.1. Determination of mean values of L_1 and t_0

The values of L_1 and t_0 are determined by a calibration run with a thin uranium foil in the incident beam and a lead sample. The spectra in the ^{6}Li back-scattering detectors contain absorption lines due neutrons in the incident beam absorbed by the uranium resonances. A typical spectrum is shown in Fig. 16.

The absorption lines are fitted to Gaussians and the values of the time delay t_0 and the total flight path $L=L_0+L_1$ is obtained from the fitted peak positions in time of flight. (The method is described in Ref. [10] and is almost identical to that used in Section 3.2 to determine t_0 and L_0.) The value of L_1 is determined from L using the value of L_0 obtained in Section 3.2. The values of L_1 are shown for the 132 back-scattering detectors in Fig. 17a and those for t_0 in Fig. 17b.

Also shown in Fig. 17a as the red circles are the values of L_1, obtained using the lead calibration run via the procedure described in Section 3.3. The two procedures are in good agreement. The values of L_1 obtained from the lead calibration are preferred as they have better statistical accuracy.

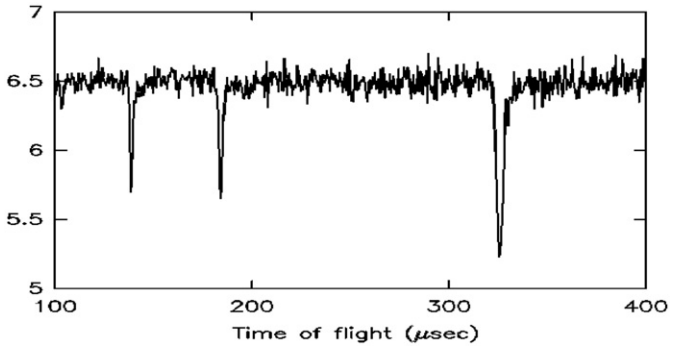

Fig. 16. A typical spectrum from one of the 132 back-scattering detectors, obtained by scattering from the lead calibration sample with a uranium foil in the incident beam. The data is divided by scattering from a lead calibration with no uranium foil to remove the spectrum shape.

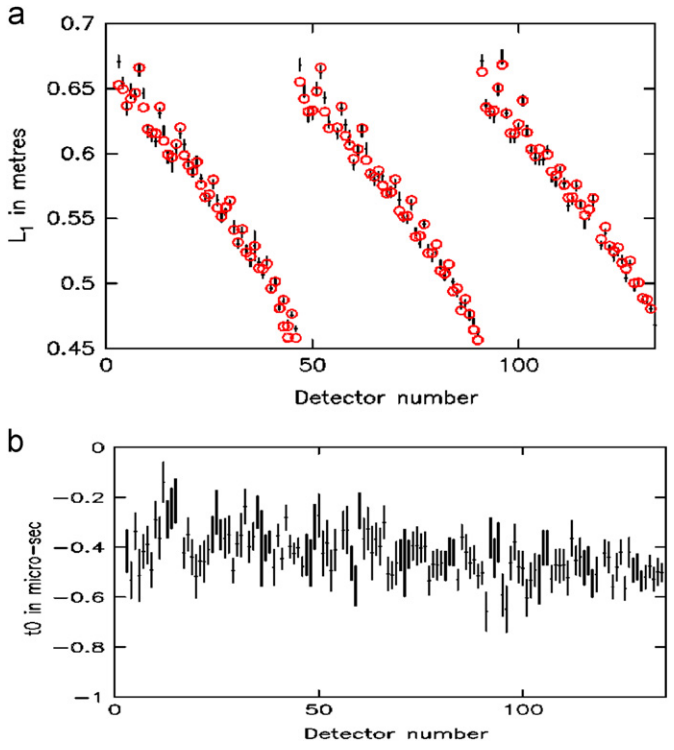

Fig. 17. (a) Shows calibrated values of L_1 for the 132 back-scattering detectors. The points with error bars were obtained using the lead calibration sample with a uranium foil in the incident beam. The red circles were obtained by fitting the positions of the lead peak with no uranium foil in the incident beam. (b) Shows calibrated values of t_0 for the 132 back-scattering detectors. (For interpretation of the references to colour in this figure legend, the reader is referred to the web version of this article.)

5.2. Determination of the resolution components Δt, ΔL_1 for ^{6}Li detectors

The values of Δt, the uncertainty in the measurement of t, and ΔL, the uncertainty in the total flight path for the ^{6}Li detectors are determined from the fitted widths of the absorption lines, illustrated in Fig. 16. The procedure used is described in Ref. [10] and is very similar to that followed in Section 4.1. Fig. 18a and b shows the values obtained for ΔL andΔt in spectra 3–135.

From the value of $\Delta L_0=2.1$ cm, obtained by the method given in Section 4.1, the uncertainty in the final flight path is determined as

$$\Delta L_1 = [\Delta L^2 - \Delta L_0^2]^{1/2} \quad (9)$$

Note that Eq. (9) makes the approximation that L_0 and L_1 have a Gaussian distribution about their mean value and that there is no correlation between these parameters. Table 4 lists the average

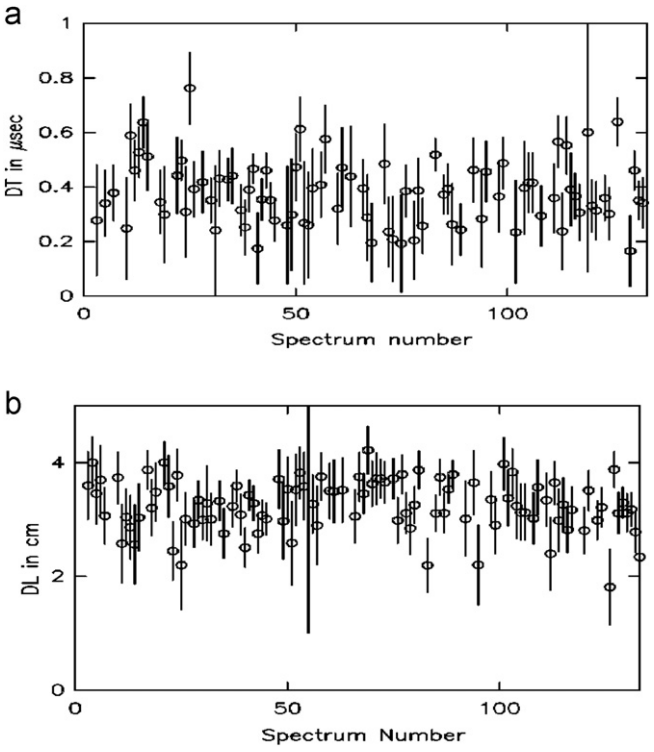

Fig. 18. (a) Values of Δt in μs for the 132 back-scattering detectors. (b) Values of ΔL in cm for the 132 ^{6}Li doped back-scattering detectors.

Table 4
List of the average values of t_0, Δt, ΔL_1 and E_1 over the three banks of 44 detectors.

Detector bank	t_0 (μs)	Δt (μs)	ΔL_1 (cm)	E_1 (meV)
S3–S46 (^{6}Li)	-0.39 ± 0.01	0.42 ± 0.02	2.2 ± 0.1	4897.1 ± 0.7
S47–S90 (^{6}Li)	-0.44 ± 0.01	0.38 ± 0.02	2.5 ± 0.1	4897.5 ± 0.7
S91–S132 (^{6}Li)	-0.49 ± 0.01	0.40 ± 0.02	2.1 ± 0.1	4895.6 ± 0.8
S135–S198 (YAP)	-0.40 ± 0.02	0.37 ± 0.02	2.2 ± 0.2	4897.3 ± 0.4

values of t_0, Δt, ΔL_1 and E_1 over the three banks of 44 detectors. Also listed for comparison are the average values obtained for the YAP detectors at forward angles in Sections 3 and 4.

6. Resolution for different masses

The VESUVIO spectrometer measures the momentum distribution of atoms. The momentum of the atoms is conventionally denoted as y and is determined by the measured time of flight t, and the instrument parameters measured by the calibration procedure described in Sections 3–5:

$$y = y(t, L_1, L_0, \theta, E_1)$$

The resolution component in momentum space due to the energy resolution width is calculated as

$$\Delta y_E = \frac{\partial y}{\partial E_1} \Delta E_1$$

where ΔE_1 is the calibrated width of the energy resolution function. The resolution components due to uncertainties in the other parameters defining the instrument are calculated similarly. The resolution widths are given in Å^{-1}. These can be converted to momentum using the de Broglie relation $p = \hbar k$.

Values of these components for in momentum space are given at forward angles for hydrogen in Fig. 19a and deuterium in Fig. 19b. For measurements with $M > 2$ the back scattering detectors give better resolution. The resolution is shown for lithium in Fig. 19c, oxygen in Fig. 19d and Pb in Fig. 19e. The resolution for ^{4}He at backscattering is given in Fig. 19f. All resolution components are assumed to be Gaussian, except for the energy resolution function, which is a convolution of a Lorentzian and a Gaussian. Quoted Gaussian widths are standard deviations while Lorentzian widths are the HWHM.

It can be seen that in all cases the resolution function is dominated by the uncertainty with which the final energy and the scattering angle are known. Generally the energy resolution is

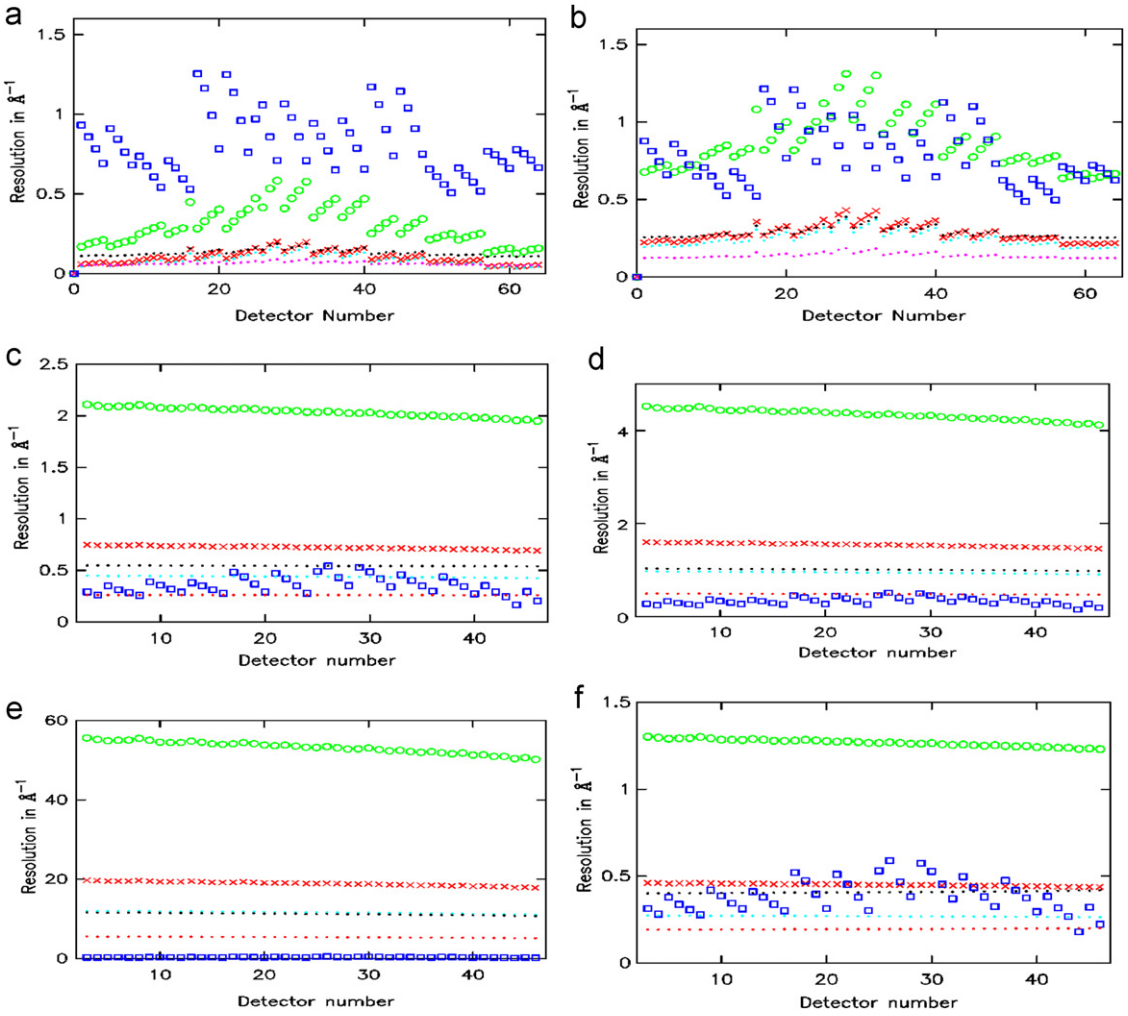

Fig. 19. (a) The resolution for scattering from H in the forward scattering YAP detectors. Typical H peak widths are in the range 3–5 Å^{-1}: blue rectangles, angular resolution; green open circles, Gaussian component of energy resolution; red crosses, Lorentzian component of energy resolution; black filled circles, component due to uncertainty in L_0; pink filled circles, component due to uncertainty in L_1; light blue filled dots, component due to uncertainty in t. (b) The resolution for scattering from D in the forward scattering bank. Typical D peak widths are in the range 4–6 Å^{-1}. (c) Resolution for ^{7}Li at back scattering with the double difference technique. Typical Li peak widths are $\sim$7 Å^{-1}: blue rectangles, angular resolution; green open circles, Gaussian component of energy resolution; red crosses, Lorentzian component of energy resolution; light blue filled dots, component due to uncertainty in L_0; black filled circles, component due to uncertainty in L_1; pink filled circles; component due to uncertainty in t. (d) Resolution for O at backscattering with the double difference method. Typical O peak widths are $\sim$10–15 Å^{-1}. (e) Resolution for Pb at back scattering with the double difference method. The width of the Pb peak at 0 K is 35 Å^{-1}: blue rectangles, angular resolution; green open circles, Gaussian component of energy resolution; red crosses, Lorentzian component of energy resolution; black filled circles, component due to uncertainty in L_0; pink filled circles, component due to uncertainty in L_1; light blue filled dots, component due to uncertainty in t. (f) Resolution for He4 at back scattering with the double difference method. Typical peak widths in liquid and solid He4 are $\sim$1 Å^{-1}. (For interpretation of the references to colour in this figure legend, the reader is referred to the web version of this article.)

dominant, but for measurements of hydrogen (which is the main application of VESUVIO) the angular resolution dominates with the current instrument geometry.

The current best resolution for measurements of hydrogen is typically ~25% of the intrinsic width due to the zero point motion of protons. For D it is ~20%, for Li ~30%, for O ~25%. Hence in these cases the shape of the momentum distribution can be measured with reasonable accuracy. For scattering from heavier elements the resolution becomes progressively worse. Liquid and solid ^{4}He and ^{3}He are a special case due to their extremely narrow momentum distributions. In these cases the resolution on VESUVIO is at present too poor to measure peak shapes and only mean kinetic energies of atoms can be determined.

7. Summary and discussion

The procedure for calibrating the VESUVIO eV neutron spectrometer at the ISIS neutron source has been described. It determines all the relevant numerical parameters required for analysis of neutron data at energy transfers in the eV region. The way in which these parameters are incorporated into routines used to determine the momentum distributions of atoms in liquids and powders is described in detail in Ref. [2].

For scattering from protons, which is the primary current application of VESUVIO, the resolution function in the proton momentum space is dominated by the uncertainty with which the scattering angle is known. This uncertainty could be much reduced by the following:

(a) Changing the current instrument geometry to circular detector rings with detector planes at a tangent to the Debye–Scherrer cone. This would eliminate the degradation of angular resolution $\Delta\theta$ for detectors which lie out of the horizontal plane in the current instrument geometry (see Fig. 15a). For some detectors this would improve resolution by a factor 2 with no loss in count rate.
(b) Moving the detectors further away. Since $\Delta\theta$ is inversely proportional to L_1, the angular resolution could be improved indefinitely, although with a corresponding drop in count rate $\propto 1/L_1^2$ on individual detectors.

At present the VESUVIO resolution is too poor to extract detailed information on the peak shapes of liquid and solid ^{3}He and ^{4}He due to the small interatomic interactions and the correspondingly very narrow widths of the momentum distributions. The current resolution is similar to the intrinsic width of the momentum distribution. However replacement of the backscattering detectors by YAP detectors and the use of uranium rather than gold foils would reduce the resolution width to ~30% of the intrinsic peak width and make such measurements possible in these important systems.

Apart from this special case the results of the calibrations show that measurements of atomic momentum distributions n(p) of atoms with masses lower than 16 amu can currently be measured with a resolution width ~25% of the intrinsic peak widths. Hence detailed information on the shape of n(p) can be extracted from the data as shown in Refs. [4–9].

References

[1] S.W. Lovesey, Theory of Neutron Scattering from Condensed Matter, vol. 1, Oxford University Press, 1984 (Section 3.4).
[2] J. Mayers, T. Abdul-Redah, J. Phys. Condens. Matter 16 (2004) 4811.
[3] A. Pietropaolo, R. Senesi, C. Andreani, et al., Phys. Rev. Lett. 100 (2008) 127802.
[4] C. Pantalei, A. Pietropaolo, R. Senesi, S. Imberti, C. Andreani, J. Mayers, C. Burnham, G. Reiter., Phys. Rev. Lett. 100 (2008) 177801.
[5] M. Adams, J. Mayers, Phys. Rev. Lett. 98 (2007) 85301.
[6] Y. Feng, C. Ancona-Torres, et al., Phys. Rev. Lett. 97 (2006) 69901.
[7] G. Reiter, C. Burnham, et al., Phys. Rev. Lett. 97 (2006) 247801.
[8] R. Senesi, A. Pietropaolo, et al., Phys. Rev. Lett. 98 (2007) 138102.
[9] D. Homouz, G. Reiter, et al., Phys. Rev. Lett. 98 (2007) 115502.
[10] A.L. Fielding, J. Mayers, Nucl. Instr. and Meth. A 480 (2002) 680.
[11] E.P. Cippo, G. Gorini, M. Tardocchi, et al., Meas. Sci. Technol. 19 (2008) 47001.
[12] M. Tardocchi, G. Gorini, et al., Rev. Sci. Instr. 75 (2004) 4880.
[13] C. Andreani, A. Pietropaolo, et al., Appl. Phys. Lett. 85 (2004) 5454.
[14] E.M. Schoonveld, J. Mayers, EM Schooneveld, J Mayers, NJ Rhodes, et al., Rev. Sci. Instr. 77 (2006) 95103.
[15] A. Pietropaolo, C. Andreani, et al., Nucl. Instr. and Meth. A 570 (2007) 498.
[16] P.A. Seeger, A.D. Taylor, R.M. Brugger, Nucl. Instr. and Meth. A 240 (1985) 98.
[17] S.F. Mughabghab, in: Neutron Cross Sections, Academic Press, Orlando, Florida, 1984.
[18] J. Mayers, C. Andreani, G. Baciocco, Phys. Rev. B 39 (1989) 2022.
[19] In press.
[20] J. Mayers, A.L. Fielding, R. Senesi, Nucl. Instr. and Meth. A 481 (2002) 454.
[21] C. Windsor, in: Pulsed Neutron Scattering, Taylor and Francis, London, 1981.
[22] A.D. Taylor, SNS moderator performance predictions, Rutherford-Appleton Laboratory Report RAL-84-120, 1984.